Experimental realization of hyperbolic dispersion metamaterial for the whole visible spectrum based on liquid crystalline phase soft template

Xiangjun Xiang,[1,3] Chengliang Yang,[1,*] Ying Zhang,[1,3] Zenghui Peng,[1] Zhaoliang Cao,[1] Haifeng Zhao,[2] Peiguang Zhang,[1] and Li Xuan[1]

[1]*State Key Laboratory of Applied Optics, Changchun Institute of Optics, Fine Mechanics and Physics, Chinese Academy of Sciences, Changchun, Jilin 130033, China*

[2]*State Key Laboratory of Luminescence and Applications, Changchun Institute of Optics, Fine Mechanics and Physics, Chinese Academy of Sciences, Changchun, Jilin 130033, China*

[3]*Universtiy of the Chinese Academy of Sciences, Beijing 100039, China*

[*]*ycldahai@ciomp.ac.cn*

Abstract: We experimentally demonstrated a metamaterial composed of hexagonal arrays of silver nanowires that exhibits hyperbolic dispersion and negative refraction in the entire visual wavelength range. The nanowires with extremely small size of 10 nm diameter and 15 nm center-to-center distance were fabricated using the reverse hexagonal liquid crystalline phase template containing $AgNO_3$ solution. Through the experiments of angle dependent reflectance for s-polarization and p-polarization, the dielectric constants were measured in several wavelengths. Calculations and experiments both show hyperbolic dispersion relations from 370 nm to 750 nm which indicates the presence of all-angle negative refraction. For all the experimental wavelengths, the permittivities of the material are in good agreement with the theoretical calculations.

OCIS codes: (160.3918) Metamaterials; (160.3710) Liquid crystals; (220.4241) Nanostructure fabrication; (260.2065) Effective medium theory.

References and links

1. R. Fisher and R. Gould, "Resonance cones in the field pattern of a short antenna in an anisotropic plasma," Phys. Rev. Lett. **22**(21), 1093–1095 (1969).
2. X. Chen, Y. Luo, J. Zhang, K. Jiang, J. B. Pendry, and S. Zhang, "Macroscopic invisibility cloaking of visible light," Nat. Commun. **2**, 176 (2011).
3. Z. Li, K. Bao, Y. Fang, Y. Huang, P. Nordlander, and H. Xu, "Correlation between incident and emission polarization in nanowire surface plasmon waveguides," Nano Lett. **10**(5), 1831–1835 (2010).
4. Z. Jacob, L. V. Alekseyev, and E. Narimanov, "Optical hyperlens: far-field imaging beyond the diffraction limit," Opt. Express **14**(18), 8247–8256 (2006).
5. J. B. Pendry, "Negative refraction makes a perfect lens," Phys. Rev. Lett. **85**(18), 3966–3969 (2000).
6. D. R. Smith, D. Schurig, J. J. Mock, P. Kolinko, and P. Rye, "Partial focusing of radiation by a slab of indefinite media," Appl. Phys. Lett. **84**(13), 2244–2246 (2004).
7. C. Simovski, S. Maslovski, I. Nefedov, and S. Tretyakov, "Optimization of radiative heat transfer in hyperbolic metamaterials for thermophotovoltaic applications," Opt. Express **21**(12), 14988–15013 (2013).
8. V. G. Veselago, "The electrodynamics of substances with simultaneously negative values of ε and μ," Sov. Phys. Usp. **10**, 509–514 (1968).
9. Z. Liu, H. Lee, Y. Xiong, C. Sun, and X. Zhang, "Far-field optical hyperlens magnifying sub-diffraction-limited objects," Science **315**(5819), 1686 (2007).
10. M. A. Noginov, H. Li, Y. A. Barnakov, D. Dryden, G. Nataraj, G. Zhu, C. E. Bonner, M. Mayy, Z. Jacob, and E. E. Narimanov, "Controlling spontaneous emission with metamaterials," Opt. Lett. **35**(11), 1863–1865 (2010).
11. J. Kim, V. P. Drachev, Z. Jacob, G. V. Naik, A. Boltasseva, E. E. Narimanov, and V. M. Shalaev, "Improving the radiative decay rate for dye molecules with hyperbolic metamaterials," Opt. Express **20**(7), 8100–8116 (2012).
12. H. N. Krishnamoorthy, Z. Jacob, E. Narimanov, I. Kretzschmar, and V. M. Menon, "Topological transitions in

#241498 Received 25 May 2015; revised 29 Jul 2015; accepted 29 Jul 2015; published 6 Aug 2015

metamaterials," Science **336**(6078), 205–209 (2012).
13. P. Evans, W. Hendren, R. Atkinson, G. Wurtz, W. Dickson, A. Zayats, and R. Pollard, "Growth and properties of gold and nickel nanorods in thin film alumina," Nanotechnology **17**(23), 5746–5753 (2006).
14. S. A. Ramakrishna, "Physics of negative refractive index materials," Rep. Prog. Phys. **68**(2), 449–521 (2005).
15. J. Elser, R. Wangberg, V. A. Podolskiy, and E. E. Narimanov, "Nanowire metamaterials with extreme optical anisotropy," Appl. Phys. Lett. **89**(26), 261102 (2006).
16. M. Scalora, G. D'Aguanno, N. Mattiucci, M. J. Bloemer, D. de Ceglia, M. Centini, A. Mandatori, C. Sibilia, N. Akozbek, M. G. Cappeddu, M. Fowler, and J. W. Haus, "Negative refraction and sub-wavelength focusing in the visible range using transparent metallo-dielectric stacks," Opt. Express **15**(2), 508–523 (2007).
17. X. Yang, J. Yao, J. Rho, X. Yin, and X. Zhang, "Experimental realization of three-dimensional indefinite cavities at the nanoscale with anomalous scaling laws," Nat. Photonics **6**(7), 450–454 (2012).
18. S. Townsend, S. Zhou, and Q. Li, "Multiscale metamaterials: a new route to isotropic double-negative behaviour at visible frequencies," Opt. Express **22**(18), 21929–21937 (2014).
19. J. Sun, J. Zhou, B. Li, and F. Kang, "Indefinite permittivity and negative refraction in natural material: Graphite," Appl. Phys. Lett. **98**(10), 101901 (2011).
20. M. A. van de Haar, R. Maas, H. Schokker, and A. Polman, "Experimental realization of a polarization-independent ultraviolet/visible coaxial plasmonic metamaterial," Nano Lett. **14**(11), 6356–6360 (2014).
21. J. Yao, Z. Liu, Y. Liu, Y. Wang, C. Sun, G. Bartal, A. M. Stacy, and X. Zhang, "Optical negative refraction in bulk metamaterials of nanowires," Science **321**(5891), 930 (2008).
22. E. Ozbay, "Plasmonics: Merging photonics and electronics at nanoscale dimensions," Science **311**(5758), 189–193 (2006).
23. P. B. Johnson and R.-W. Christy, "Optical constants of the noble metals," Phys. Rev. B **6**(12), 4370–4379 (1972).
24. Y. Liu, G. Bartal, and X. Zhang, "All-angle negative refraction and imaging in a bulk medium made of metallic nanowires in the visible region," Opt. Express **16**(20), 15439–15448 (2008).
25. A. Sihvola, *Electromagnetic Mixing Formulas and Applications* (The Institution of Engineering and Technology, 1999).
26. P. Ekwall, L. Mandell, and K. Fontell, "Solubilization in micelles and mesophases and the transition from normal to reversed structures," Mol. Cryst. Liq. Cryst. (Phila. Pa.) **8**, 157–213 (1969).
27. L. M. Huang, H. T. Wang, Z. B. Wang, A. Mitra, K. N. Bozhilov, and Y. S. Yan, "Nanowire arrays electrodeposited from liquid crystalline phases," Adv. Mater. **14**(1), 61–64 (2002).
28. A. Poddubny, I. Iorsh, P. Belov, and Y. Kivshar, "Hyperbolic metamaterials," Nat. Photonics **7**(12), 948–957 (2013).
29. M. Noginov, Y. A. Barnakov, G. Zhu, T. Tumkur, H. Li, and E. Narimanov, "Bulk photonic metamaterial with hyperbolic dispersion," Appl. Phys. Lett. **94**(15), 151105 (2009).
30. D. R. Smith and D. Schurig, "Electromagnetic wave propagation in media with indefinite permittivity and permeability tensors," Phys. Rev. Lett. **90**(7), 077405 (2003).
31. K.-T. Tsai, G. A. Wurtz, J.-Y. Chu, T.-Y. Cheng, H.-H. Wang, A. V. Krasavin, J.-H. He, B. M. Wells, V. A. Podolskiy, J.-K. Wang, Y. L. Wang, and A. V. Zayats, "Looking into meta-atoms of plasmonic nanowire metamaterial," Nano Lett. **14**(9), 4971–4976 (2014).
32. J. Zhang, Y. Yan, X. Cao, and L. Zhang, "Microarrays of silver nanowires embedded in anodic alumina membrane templates: size dependence of polarization characteristics," Appl. Opt. **45**(2), 297–304 (2006).

1. Introduction

Metamaterials which can be engineered by properly designed structural units, have become more and more important for engineering electromagnetic space and controlling light propagation. One class of metamaterials is highly anisotropic media that have hyperbolic dispersion relations, whose permittivity and permeability tensors are negative along only one principal axis of the metamaterials. The hyperbolic dispersion metamaterial (HDM) was first experimentally demonstrated in a magnetized plasma in 1969 [1]. The HDMs have shown lots of new physical phenomena and applications, including cloaking [2], optical waveguide [3], imaging [4], superlens [5], focusing [6], heat transport [7] and negative refraction [8] which may be the most practical design of HDMs. At present, the most common realizations of hyperbolic metamaterials are layered metal-dielectric structures and nanowire arrays which have been extensively studied theoretically and experimentally [9, 10]. Different metal/dielectric pairs of layered metal-dielectric structures have been demonstrated such as Au/Al_2O_3 [11], Ag/TiO_2 [12]. The standard method to fabricate nanowire arrays is electrochemical deposition of a metal on a porous alumina membrane created by anodization [13]. The properties of HDMs mainly depend on the geometry of their basic units, rather than their chemical composition [14]. When the size of basic units is much smaller than the

#241498 Received 25 May 2015; revised 29 Jul 2015; accepted 29 Jul 2015; published 6 Aug 2015

incident wavelength, the structure can be characterized as indefinite media [15]. The basic units with smaller size are favorable for realizing HDMs in wider spectral range. Thus in order to realize the HDM in the visual frequencies, the cells should be small enough, and many researchers developed a variety of structures and new fabrication methods during the last decades, such as transparent metallo-dielectric stacks [16], arrays of metal–dielectric nanopyramids [17], multiscale metamaterials [18], natural graphite [19].

Since the metamaterial structure is relatively small, the barrier associated with the fabrication difficulties is greatly increased. At present, the fabrication techniques of HDMs are mainly top-down and bottom-up methods. By the top-down method, M.A.van de Haar *et al.* fabricated silicon coaxes with a well-defined diameter in the range of 150 −168 nm with extremely thin sidewalls (13 - 15 nm), embedded in a silver film, using a combination of electron beam lithography, physical vapor deposition, reactivation etching, and focused ion beam polishing. The HDM shows a negative mode index between 440 nm and 500 nm [20]. The minimum size of the nanostructures is typically limited by resolution of the lithographic tools or the etching apparatus, and such top-down fabrication method is complicated, time-consuming and expensive. In bottom-up way, Zhangxiang *et al.* fabricated the silver nanowires (60 nm wire diameter and 110 nm center-to-center distance) by electrochemical depositing in a rigid porous alumina template, and hyperbolic dispersion was obtained by the silver nanowires at 660 nm [21]. For wire metamaterials operating at optical frequencies, it relies on the plasma resonance in the desired wavelength range. In such anisotropic material, the components of the permittivity tensor along and perpendicular to the nanowire axis with opposite signs will lead to a hyperbolic dispersion material. Taking the simple structure of the nanowires into account, the fabrication difficulties is greatly reduced, but new templates and fabrication methods still have to be studied in order to fabricate metamaterials with even smaller unit cells easily.

In this work, we employ a novel method to fabricate the HDMs with extremely small unit cells. The reverse hexagonal lyotropic crystalline is used as a soft template to fabricate silver nanowire arrays with 10 nm diameter and 15 nm center-to-center distance. Using the effective medium approximation, the permittivity is calculated with the structure parameters obtained by scanning electron microscopy (SEM). The dielectric constant of the material is measured experimentally through the polarization dependent relations of the incident angles and reflectivity. Hyperbolic dispersion is achieved in analytical calculations and experiments. As expected, the values of the experiment are very close to the calculations at measured wavelengths (410, 532, 633, 730 nm). Furthermore this fabrication method is simple, cheap and fast which also can be extended to fabricate nanostructures of other metals.

2. Hyperbolic dispersion of metallic nanowires

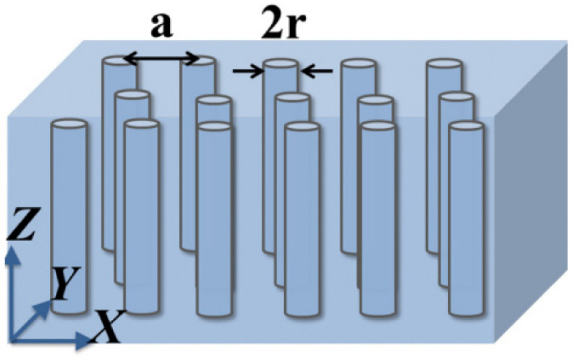

Fig. 1. Effective uniaxial metamaterial geometry of hexagonal silver nanowires array. The coordinate system is in the lower-left corner. The nanowires are parallel with Z axis.

#241498 Received 25 May 2015; revised 29 Jul 2015; accepted 29 Jul 2015; published 6 Aug 2015

One of the most common structures used to realize an HDM is the metallic nanowires arrays embedded in a dielectric matrix. Nanowire arrays have been extensively studied and various interesting effects have been demonstrated. Due to the simple structure, low loss and easy fabrication, nanowire arrays are usually chosen to achieve hyperbolic dispersion metamaterial for the optical spectrum. Figure 1 schematically illustrates the structure of nanowires arrays in hexagonal lattices. Considering the composition, the Drude model is used to describe the permittivity of silver partially in visible [22], and the Johnson-Christy data is used in the range 350nm – 550nm [23].

$$\varepsilon_m(\omega) = \varepsilon_\infty - \frac{\omega_p^2}{\omega(\omega + i\gamma_c)}. \tag{1}$$

Where the high frequency bulk permittivity $\varepsilon_\infty = 6$, the bulk plasmon frequency $\omega_p = 1.5 \times 10^{16}$rad/s, and the collision frequency $\gamma_c = 7.73 \times 10^{13}$rad/s [24].

When the radius (r) of nanowire and the distance (a) between wires are much smaller than the wavelength (λ_0) of the incident light, the nanowire arrays could be considered as an effective uniaxial material. According to Maxwell-Garnett theory [25], the permittivity parallel to wires ($\varepsilon_{//}$) and perpendicular to wires ($\varepsilon_\perp$) can be described by the following formulas:

$$\varepsilon_{\parallel} = \varepsilon_z = f\varepsilon_m + (1-f)\varepsilon_d. \tag{2}$$

$$\varepsilon_\perp = \varepsilon_x = \varepsilon_y = \varepsilon_d \left[\frac{(1+f)\varepsilon_m + (1-f)\varepsilon_d}{(1-f)\varepsilon_m + (1+f)\varepsilon_d} \right]. \tag{3}$$

Here $f = 2\pi r^2 / (\sqrt{3}a^2)$ is the filling ratio of metal; ε_m and ε_d are the permittivities of metal and dielectric. The effective parameters $\varepsilon_{//}$ and $\varepsilon_\perp$ will be calculated by Eqs. (2) and (3) below in the experimental section. When the dielectric constant Re ($\varepsilon_{//}$) <0 and Re ($\varepsilon_\perp$)>0, the dispersion relation of the nanowire arrays becomes hyperbolic.

3. Fabrication and characterization

Although the fabrications of nanowire metamaterials have been extensively studied, it is still a great challenge for large area fabrication with ultra-small unit cells. In order to fabricate ultra-small nanowires, the reverse hexagonal liquid crystalline phase is prepared as the soft template according to the phase diagram of Aerosol OT-p-xylene-water system [26].

3.1 Materials

Anionic surfactant sodium bis (2-ethylhexyl) sulfosuccinate (AOT) (98 wt %), silver nitrate (99 wt %) and oil phase p-xylene (99 wt %) were purchased from Sigma-Aldrich Chemical Company. AOT ($C_{20}H_{37}NaO_7S$) is an amphiphilic compound which contains hydrophilic heads and hydrophobic tails. Therefore, it is soluble in water and organic solvents mixture. All chemicals were used as received without further purification. Deionized water was obtained from the Millipore Elixir 100 and the resistivity is over 18 MΩ·cm.

#241498 Received 25 May 2015; revised 29 Jul 2015; accepted 29 Jul 2015; published 6 Aug 2015

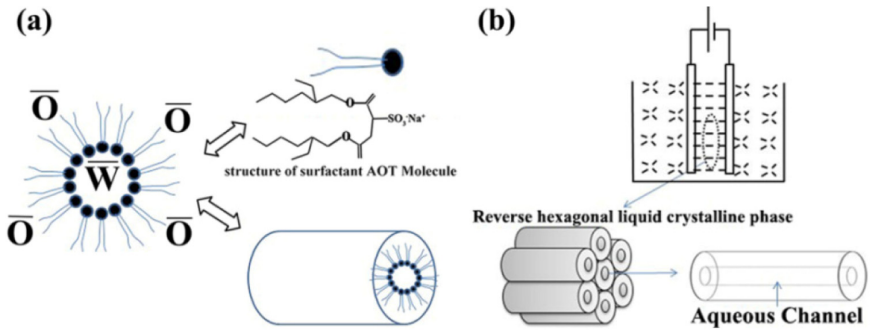

Fig. 2. The structure of AOT molecule and self-assembly alignment of reverse hexagonal liquid-crystalline phase during nanowire electrodeposition. (a) Aerosol OT ($C_{20}H_{37}NaO_7S$) is an amphiphilic compound, which contains hydrophilic head (black dot) and hydrophobic tails (the two gray curves). W and O represent water phase and oil phase, respectively. In the Aerosol OT-xylene-water system, reversed hexagonal mesophase is formed in a special composition. The hydrophilic heads of Aerosol OT arrange inwardly contact with water, and the hydrophobic tails attach to the outside oil. (b) Schematic illustration of the silver nanowires electrodeposition. The narrowly separated electrodes create an electric field high enough to align the reverse hexagonal liquid crystal parallel to the electric field direction. The water phase is substituted by an aqueous 0.3 M $AgNO_3$ solution in this experiment.

3.2 Preparation of reverse hexagonal liquid-crystalline phases and electrodeposition

We employed the reverse hexagonal liquid-crystalline phase as a soft template. Figure 2(a) shows the molecular structure of Aerosol OT and the schematic illustration of self-assembly. Aerosol OT contains one hydrophilic head and two hydrophobic tails. The hydrophilic heads of Aerosol OT arrange inwardly contact with H_2O, and the hydrophobic tails attach to the outside p-xylene. The aqueous solution of silver nitrate is isolated in the channels which are arranged in hexagon due to the self-assembly effect. P-xylene played a role of separator around the channels. As electrochemical reactions just occur in the aqueous channels, silver nanowires were produced on the negative electrode. In the reverse hexagonal liquid-crystalline phase, different compositions result the different geometrical sizes of aqueous channels of template. The period and diameter of the nanowires can be easily regulated by controlling the aqueous channels of template with different compositions. For growth of silver nanowire arrays, a specific composition was used in our experiment which is 1.4 M AOT in p-xylene, 10 molar ratio of [H_2O]/ [AOT], and an aqueous 0.3 M $AgNO_3$ solution replacing the water phase. The mixture was kept in a black bottle to avoid direct light exposure during the entire experiment process, and it was stirred for 2h until it turned to be clear and transparent liquid. Then it was kept to equilibrate for 20min in the 5°C water bath before electrodeposition. Figure 2(b) shows the experiment setup of electrodeposition. A silver foil (2.0 mm 99%) which was from Alfalfa Aesar was used as the positive electrode. An indium tin oxide (ITO) glass (5.0*8.0 mm^2) was used as negative electrode to collect the nanowires whose surface was very smooth and clean. The electrodes were bonded by epoxy-resin adhesive with the distance about 0.7mm. The mixture liquid was used as the electrolyte, and the electrodeposition was performed with a DC power supply. The reverse hexagonal liquid crystalline phase could be aligned parallel to the electric field. As a result, the high-density nanowire arrays grew perpendicular to the electrode [27]. Static potential of 3.0V was applied for 30min at the temperature of 5.0°C in the electrodeposition. After the electrodeposition, the negative electrode ITO glass was softly washed by ethanol and ultrasonic cleaning.

3.3 Characterization (SEM and EDX analysis)

The nanowire metamaterial fabricated in this work is made of aligned silver nanowires which vertically stand on the ITO glass. Figure 3(a) shows a photograph of the sample. The gray

#241498 Received 25 May 2015; revised 29 Jul 2015; accepted 29 Jul 2015; published 6 Aug 2015

layer is the silver nanowires we fabricated, which are attached to the ITO glass. From Fig. 3(a) we can see that the material is quilting uniform in centimeter scale. Figure 3(b) shows the SEM micrograph of the high-density aligned nanowires on the ITO glass. The fabricated sample was characterized by FE-SEM S-4800 from HITACHI. The white area represents silver and dark background is the glass. As can be seen, the nanowires arrange in the hexagonal form. These nanowires have a mean diameter of 10 nm, center-to-center distance of 15 nm. As the template is a kind of soft template which forms the aqueous channels by self-assembly effect, the degree of order for the template will decrease with the length of aqueous channel increasing. So the length of silver nanowire array is typically limited in several micrometers. For actual metamaterials, the inverse of structural elements size represents an upper limit for the magnitude of wave vectors [28]. So the smaller element size is favorable for realizing hyperbolic isofrequency surfaces for wide wave-vector range.

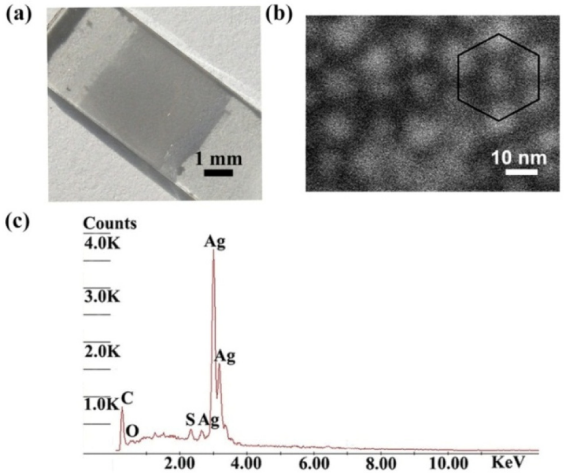

Fig. 3. (a) The photograph of the nanowires sample. (Scale bar, 1mm) (b) Scanning electron micrographs of the material electrodeposited from AOT/p-xylene/H_2O (0.3M $AgNO_3$) reverse hexagonal liquid-crystalline phase. Silver appears as white parts surrounded by dark background, and the silver nanowires are arranged in hexagonal form (black line). The average diameter is about 10nm, nanowires spacing is about 15nm. (Scale bar, 10nm) (c) Energy dispersive X-ray of the sample. The elements consist C, O, S, Ag; the main component of the sample is Ag and the other elements can be attributed to the AOT left in the sample.

The EDX spectrum of the sample is shown in Fig. 3(c), and it reveals that the materials are mainly composed of metallic silver. The Ag peak can be attributed to silver nanowires; the other detected peaks (C, O, and S) can be attributed to the liquid crystal template left in the sample. Owing to the nano-scale space between the nanowires, the template molecule cannot be completely removed from the array by the simple washing process.

4. Experiments and calculations

We apply an efficient method to verify the hyperbolic dispersion of the fabricated material by measuring the angle dependent reflectance of S and P polarized beam [29]. Follows are the relations between the incident angle and the reflectivities of S and P polarized beam.

$$R_s = |r|^2 = \left|\frac{\sin(\theta_i - \theta_t)}{\sin(\theta_i + \theta_t)}\right|^2, \theta_t = arc\sin\left(\frac{\sin\theta_i}{\sqrt{\varepsilon_\perp}}\right). \tag{4}$$

$$R_p = |r|^2 = \left|\frac{\varepsilon_\perp \tan\theta_t - \tan\theta_i}{\varepsilon_\perp \tan\theta_t + \tan\theta_i}\right|^2, \theta_t = \arctan\sqrt{\frac{\varepsilon_{//}\sin^2\theta_i}{\varepsilon_{//}\varepsilon_\perp - \varepsilon_\perp \sin^2\theta_i}}. \tag{5}$$

#241498 Received 25 May 2015; revised 29 Jul 2015; accepted 29 Jul 2015; published 6 Aug 2015

Here θ_i and θ_t are incident angle and refractive angle, R_S and R_P are reflectivities of S and P polarized light, the permittivity parallel to wires is $\varepsilon_{//} = \varepsilon_z$ and perpendicular to wires is $\varepsilon_\perp = \varepsilon_x = \varepsilon_y$, respectively. We measured the relations between incident angles and reflectivities for S and P polarizations. It is obvious that R_S is related to $\varepsilon_\perp$, R_P is related to both $\varepsilon_\perp$ and $\varepsilon_{//}$, according to Eqs. (4) and (5). Firstly, we measured the value of $\varepsilon_\perp$ by fitting the reflectivity curve of S polarization. Secondly, the $\varepsilon_\perp$ was taken as a known value to fit the reflectivity curve of P polarization with $\varepsilon_{//}$ as variable. The effective permittivity tensor of the nanowire arrays was retrieved. Using the parameters of the sample in Fig. 3(b), the permittivity tensor also could be calculated according to Eqs. (2) and (3).

The experimental setup is shown in Figs. 4(a) and 4(b). Several wavelengths (λ = 410, 532, 633, 730 nm) solid-state lasers are used as the light source, which almost cover the entire visible spectrum. A half-wave plate and a polarizer are used to adjust the light intensity continuously and control the polarization of the light. The spot of incident light on the sample should be small in order to measure the reflectivity accurately at large incident angle. As the beam is divergent, a lens with 200 mm focal length is used to focus the incident beam which guarantees that all incident beams can be reflected by the sample especially for the large rotation angle and all reflected energy can be received by the detector. For achieving the continuous and accurate rotation of the sample, a rotary stage driven by a stepper motor is used. A Lab Max-top laser power meter from Coherent is used at the end to measure the power of reflected beam.

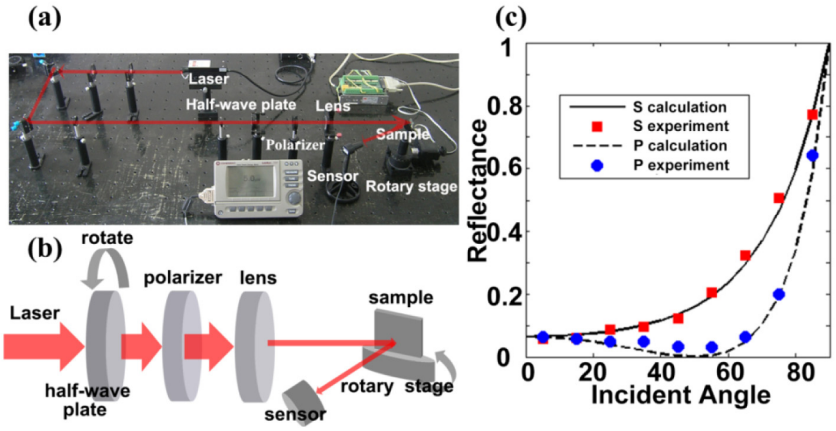

Fig. 4. Experimental setup and reflectivity measurement results. (a) The photograph of the experiment setup. (b) The schematic of experimental setup used in the reflectance measurements. A half-wave plate and a polarizer are used to adjust the light intensity continuously. A polarizer is used to control the polarization state of the light. The sample is attached on the rotary stagy.(c) The relations between the reflectivity and the incident angle in s-polarization (red squares) and p-polarization (blue circles) at 532nm wavelength. The lines are fitting curves according to Eqs. (4) and (5) and the discrete dots are experimentally measured data. The fitting effective permittivities of the sample are $\varepsilon_{//} = -3.95$ and $\varepsilon_\perp = 2.96$ respectively.

Figure 4(c) shows the relations between reflectivity of the sample and the incidence angles at 532 nm. The discrete dots are experimentally measured values; the lines are fitted curves according to Eqs. (4) and (5). For S-polarization, the reflectance increases as the incident angle increases. As expected, the curve agrees with the measured values very well. The measured fitting value is $\varepsilon_\perp = 2.96$ (calculated value is 2.84 according to the Johnson-Christy data). As for P-polarized light, the reflectance decreases nearly to zero firstly, then quickly increases as the incident angle increases. According to the experimentally measured data the Brewster angle is about 50 degrees, which is also well consistent with the calculated values (50.5 degrees). The experimentally measured values are slightly larger than zero near the

#241498 Received 25 May 2015; revised 29 Jul 2015; accepted 29 Jul 2015; published 6 Aug 2015

Brewster angle which is because the beam is not purely P-polarized after the polarizer in the experiment. However, the overall fitting curve corresponds well with the measured values. The measured fitting value is $\varepsilon_{//} = -3.95$ which is close to the calculated value –4.12.

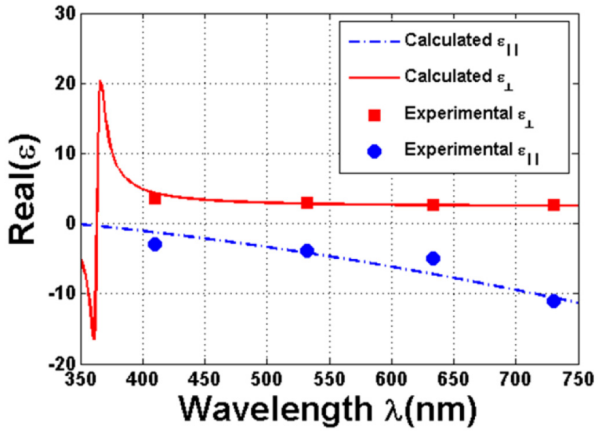

Fig. 5. The calculated and experimentally measured effective permittivities of the sample. The red solid line is the real part of the permittivity perpendicular to the silver wires and the blue dotted line is the permittivity parallel to the wires, the two lines are calculated by solving the Maxwell-Garnett equations. For the red solid line, a resonant peak appears around 370 nm, and the values keep positive in the longer wavelength. To the contrary, the blue dotted line is negative in the whole 350 nm to 750 nm spectrum. The experimental results ($\varepsilon_{\perp}$ red square and $\varepsilon_{//}$ blue circle) show the measured values from the reflectivity experiment at 410, 532, 633, 730 nm. The experiment data agree well with the calculated data.

To further investigate the hyperbolic dispersion in visual wavelength, the permittivities of the sample are calculated in the whole visual spectrum and experimentally measured at 410, 532, 633, 730 nm. Figure 5 shows the relations between wavelength and permittivities of the sample. The red squares and blue circles are experimental data from the reflectivity measurement. The red solid and blue dashed lines are the calculated dispersion diagrams which are obtained by solving Maxwell-Garnett equations Eqs. (2) and (3) and the Johnson-Christy data for hexagonal silver nanowire arrays. The experimental data agree well with the calculated curves. The effective permittivity of the metamaterial shows that the dielectric constant Re ($\varepsilon_{//}$) <0 and Re ($\varepsilon_{\perp}$)>0 are achieved in the wavelengths longer than 370 nm, which means that the hyperbolic dispersion occurs in the whole visible spectrum. As expected, negative refraction could be achieved in the visible wavelength range [30]. Due to the extremely small units and high density of the nanowires, coupling of the incident wave to surface plasma polaritons results in the epsilon-near-zero (ENZ) condition shifting to the wavelength of 350 nm The effective permittivity spectrum has a dominant peak at the wavelength of 370 nm, which is related to the resonant electron oscillations perpendicular to the nanowire axes [31].

According to the Maxwell-Garnett theory, the optical response wavelength of the metamaterial can be modulated by the filling ratio of the metal nanowires in the dielectric matrix. The medium around the silver nanowires causes the fluctuation of effective permittivity throughout the material, which leads to deviation of property from design [32]. When the surrounding medium is replaced with liquid crystal, it is convenient to modify the anisotropic permittivity of material by applying electric field to control the orientation of liquid crystal molecule. Moreover, the diameter of aqueous channels also can be adjusted by changing the molar ratio of [p-xylene]/ [H_2O]/ [AOT]. Since the radius of silver nanowires is closely related to the aqueous channels, it is able to control the filling ratio through the molar ratio. By this way, we can fabricate materials with particular permittivity by adjusting molar ratio of template.

#241498 Received 25 May 2015; revised 29 Jul 2015; accepted 29 Jul 2015; published 6 Aug 2015

5. Conclusion

In summary, we employ the liquid crystalline phase template to fabricate hyperbolic dispersion metamaterials which can realize negative refraction in the whole visible frequencies. The HDMs consisting silver nanowire arrays are electrodeposited in the soft template, which are the reverse hexagonal liquid-crystalline phase containing aqueous channels. Hyperbolic dispersion is achieved both in theoretical calculations and experiments in the 370 −750 nm spectrum. The experimentally measured permittivity agrees well with the calculated values in the measured wavelengths. Such materials may have potential applications in subwavelength imaging, superlens, heat transport and optical waveguide. Moreover, such fabrication method is fast, inexpensive, and suitable to fabricate large size uniform materials.

Acknowledgments

This work is supported by the National Natural Science Foundation of China, with grant numbers 11204299, 61205021.

#241498 Received 25 May 2015; revised 29 Jul 2015; accepted 29 Jul 2015; published 6 Aug 2015